EUROFUSION WPHCD-PR(16) 16023

P. Kalaria et al.

Systematic cavity design approach for a multi-frequency gyrotron for DEMO and study of its RF behavior

Preprint of Paper to be submitted for publication in
Physics of Plasmas

This work has been carried out within the framework of the EUROfusion Consortium and has received funding from the Euratom research and training programme 2014-2018 under grant agreement No 633053. The views and opinions expressed herein do not necessarily reflect those of the European Commission.

Systematic cavity design approach for a multi-frequency gyrotron for DEMO and study of its RF behavior

P C Kalaria[1], K A Avramidis[1], J Franck[1], G Gantenbein[1], S Illy[1], I Gr Pagonakis[1], M Thumm[1,2] and J Jelonnek[1,2]
[1]Institute for Pulsed Power and Microwave Technology (IHM),
[2]Institute of High Frequency Techniques and Electronics (IHE),
Karlsruhe Institute of Technology (KIT), Karlsruhe, Germany.

E-mail: parth.kalaria@partner.kit.edu

Abstract. High frequency (>230 GHz) megawatt-class gyrotrons are planned as RF sources for electron cyclotron resonance heating and current drive (ECRH&CD) in DEMOnstration fusion power plants (DEMOs). In this paper, for the first time, a feasibility study of a 236 GHz DEMO gyrotron is presented by considering all relevant design goals and the possible technical limitations. A mode-selection procedure is proposed in order to satisfy the multi-frequency and frequency-step tunability requirements. An effective systematic design approach for the optimal design of a gradually tapered cavity is presented. The RF-behavior of the proposed cavity is verified rigorously, supporting 920 kW of stable output power with an interaction efficiency of 36 % including the considerations of realistic beam parameters.

1. Introduction

Gyrotrons are the most prominent sources of millimeter, sub-millimeter and terahertz waves with a very high power ranging from several kW to well above 1 MW. In plasma experiments relevant to magnetically confined fusion research, gyrotrons are used as efficient, high-frequency (100 – 300 GHz) RF sources for Electron Cyclotron Resonance Heating and Current Drive (ECRH&CD) [1]. High-power microwave beams are also a means to mitigate instabilities in magnetically confined plasmas. Presently, in the Wendelstein 7-X (W7-X) stellarator facility in Greifswald (Germany), ten gyrotrons, each emitting 1 MW CW (1800s) at 140 GHz, are successfully installed to deliver sufficient ECRH power for steady-state plasma operation, in addition to Ion Cyclotron Resonance Heating (ICRH) and Neutral Beam Injection (NBI) heating [2]. For ECRH&CD applications in the ITER tokamak in Cadarache (France), 24 MW of long-pulse (~3600 s) RF power at 170 GHz is needed, which is planned to be generated from 24 × 1 MW gyrotrons [3-7]. After successful operation of ITER, it is proposed to build a DEMOnstration power plant (DEMO), which will be the first prototype of commercial fusion power plants. ECRH&CD by gyrotrons is currently considered to be a mature auxiliary heating system for DEMO [8].

As per the European Union 2012 DEMO baseline (tokamak aspect ratio = 4.0), the detailed design goals for a DEMO gyrotron together with today's technological constraints are listed in Table 1. (As will be discussed later on, the possibility of multi-frequency operation in steps of 30-40 GHz makes this table relevant also for the recently updated EU 2015 DEMO baseline with tokamak aspect ratio = 3.1). To achieve a high energy gain in the fusion power plant, a total gyrotron efficiency of more than 60 % is desired, e. g. with the help of a multi-stage depressed collector. This requirement also suggests a minimum interaction efficiency of 35 %. To reduce the total number of tubes required for sufficient ECRH&CD power, RF output power per gyrotron shall be as high as reasonably possible. The expected output power per gyrotron is around 1 MW in the case of a hollow-cavity gyrotron, which is the focus of this work, whereas it might be increased to around 2 MW in case of more complex, coaxial-cavity gyrotrons, according to feasibility analyses undertaken at the Karlsruhe Institute of Technology (KIT) [9]. It is beneficial to use the same gyrotron as a multi-purpose tube in a fusion facility, with respect to the various operational stages, which require different microwave frequencies

(e. g. plasma start-up, non-inductive current drive, and bulk heating). Furthermore, the same operational stage in facilities with different torus aspect ratios would require different microwave frequencies, as indicated in [10-12]. It is understood that the above mentioned requirements can be fulfilled by a proper "multi-frequency" gyrotron design. It should be noted that such a design is possible using the usual single-disk CVD windows and quasi-optical output couplers. In addition to multi-purpose capability, frequency-step tunability in steps of 2 – 3 GHz is necessary for plasma stabilization using fixed ECCD launchers in the fusion plasma vessel.

Table 1. Design goals and technological constraints for EU DEMO gyrotrons.

Goals	
Frequency	230 – 240 GHz
Output power	~ 1 – 2 MW
Total gyrotron ("plug-in") efficiency	> 60 %
Beam-wave interaction efficiency	> 35 %
Frequency step for fast tunability	2 – 3 GHz
Frequency step (slow) for multi-frequency operation	30 – 40 GHz
Constraints	
Peak ohmic wall loading at cavity	≤ 2 kW/cm^2
Cathode emitter current density	≤ 4 A/cm^2
Electric field at cathode	≤ 7 kV/mm
Width of electron beam	≤ λ/5
Emitter radius	~ 50 – 70 mm

At KIT, various new approaches and concepts which can contribute to fulfill the technical requirements for DEMO gyrotrons are under study, such as a multi-stage depressed collector (MSDC) design for higher efficiency [13], an advanced magnetron injection gun (MIG) design to generate optimum electron beam for high frequency operations [14], an improved quasi-optical launcher design for higher Gaussian content of the output beam [15-16], etc. The construction of a sophisticated test stand for advanced gyrotrons, called FULGOR (Fusion Long Pulse Gyrotron Laboratory), is also ongoing at KIT [17].

In this work, a possible hollow cavity, high-power 236 GHz DEMO gyrotron is investigated with the consideration of the mentioned specifications and technical limitations. The rest of the paper is structured as follows: In section 2, the main factors for the mode selection of the DEMO gyrotron are discussed along with finalized mode series concerning multi-frequency, multi-purpose operation and frequency-step tunability. Based on that, our systematic cavity design approach is presented in Section 3. The RF behavior and mode stability of the finalized cavity are discussed in Section 4. This work is concluded in Section 5.

2. Mode selection for the multi-purpose, frequency-step tunable DEMO gyrotron

In accordance with the statements above, our main considerations for mode selection of the DEMO gyrotron are: peak ohmic loading on the cavity wall, mode competition, multi-frequency operation for multi-purpose applications and frequency-step tunability. In this section, each of these aspects are discussed in detail.

2.1 Limitations of cavity wall loading and mode competition

The cavity wall loading scales with $f^{5/2}/[\chi_{m,p}{}^2 \cdot (1-(R_{caustic}/R_{cavity})^2)]$, where f is the operating frequency of the gyrotron, χ_{mp} is the p^{th} root of the derivative of the Bessel function J_m(x), (this is is the eigenvalue of the operating mode TE$_{m,p}$, where m and p is the azimuthal and the radial index of the mode, respectively), and $R_{caustic}/R_{cavity} = m/\chi_{m,p}$ is the relative caustic radius of the mode [10]. Due to this condition, maintaining the wall loading below the acceptable limit at high operating frequency (>200 GHz) is only possible when modes with high eigenvalues and/or small caustic radii are used, that

is, asymmetric, high-order volume modes ($m >> 1$, $p > 2$) with relative caustic radius less than 0.5. As compared to the "whispering gallery" $TE_{m,p}$ modes (with $m >> p$), these modes suffer less from high wall loading. Since gyrotrons operate with transversal electric modes close to cutoff, the cavity (interaction section) radius R_{cavity} can be estimated using the formula for cutoff frequencies in circular waveguides:

$$R_{\text{cavity}} \cong (c \cdot \chi_{m,p})/(2 \cdot \pi \cdot f) \quad (1)$$

Here, c is the speed of light. As will be derived below, the corresponding eigenvalue of the selected mode should be larger than 95 to fulfill the requirements in Table 1.

As the mode eigenvalue increases, the mode spectrum becomes denser. In the case of operating modes with very high eigenvalue, it becomes increasingly difficult to excite desired operating mode during start-up due to the competing modes. However, these dense mode spectra are nearly identical for nearby modes. As an example, in Figure 1, the coupling factor, as defined in [18], of an ideal electron beam to modes around $TE_{-43,15}$ and $TE_{-44,15}$ is shown. (In this work, the modes co-rotating with the beam electrons are represented with a negative sign, while counter-rotating modes are presented with a positive sign.) Both mode spectra are nearly identical in the region of interest, which makes the selection of one particular high-order mode from a suitable area in the m-p plane less relevant than in the case of lower-order modes. This has already been acknowledged in [19]. This particular feature prompts mode selection according to additional criteria like multi-frequency operation and frequency tunability, which is restricted by the RF window design and the design of the quasi-optical launcher. This is presented in the next section.

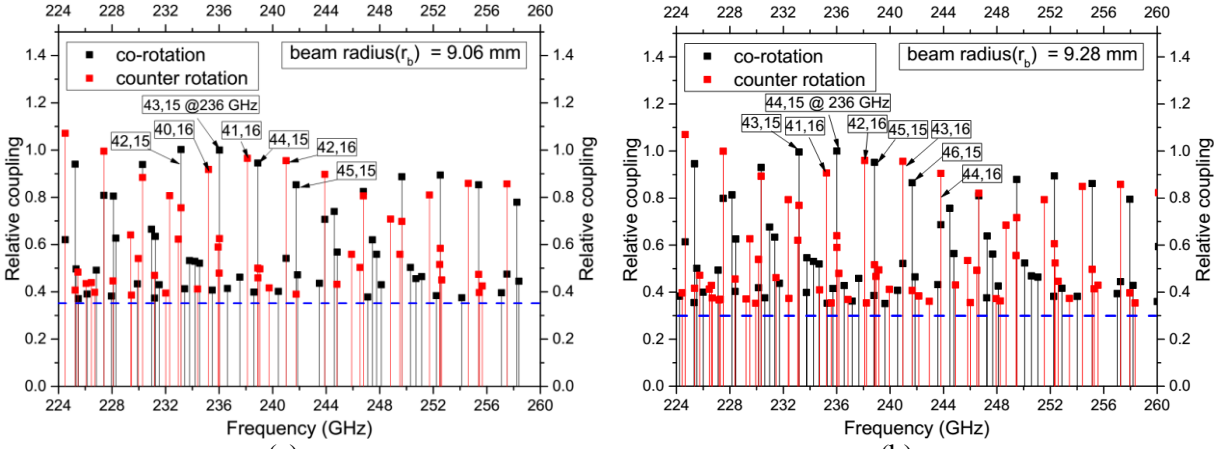

Figure 1. Mode spectra around the cavity operating mode (a) $TE_{43,15}$ (eigenvalue 103.21) and (b) $TE_{44,15}$ (eigenvalue = 104.46) at 236 GHz and for cavity radius 20.88 mm and 21.14 mm, respectively. Within the range of -5 % to +10 % of the center frequency of 236 GHz, all neighboring modes with relative coupling factor higher than 35% are plotted.

2.2 Mode selection considering multi-frequency, multi-purpose operation

As discussed in Section 1, multi-frequency operation of gyrotrons is desired for multi-purpose applications. To support this, the selected operating frequencies must correspond to the reflection minima of a single disk window, according to

$$f_N = \frac{c}{2 \cdot d \cdot \sqrt{\varepsilon_r}} \cdot N = f_B \cdot N \quad (2).$$

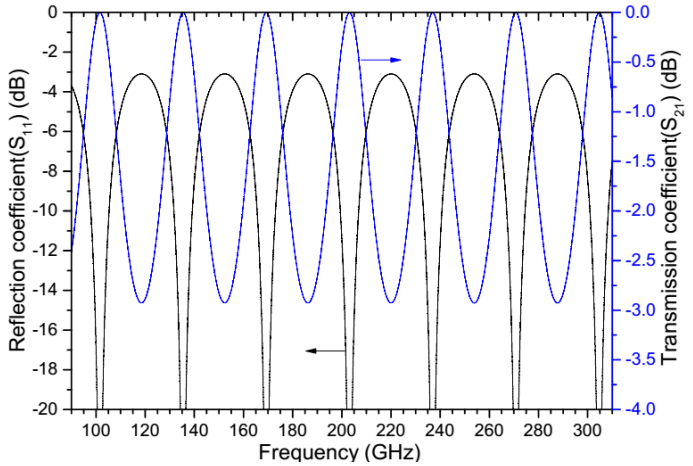

Figure 2. Calculated reflection coefficient (S_{11}) and transmission coefficient (S_{21}) of a single disk CVD-diamond window ($\varepsilon_r = 5.67$) using an in-house scattering matrix code. Window thickness = 1.861 mm. Frequency range: 90 GHz to 310 GHz.

Here, d is the window thickness and N is an integer. The minimum and maximum disk thickness can be determined by considering mechanical stability and cost. The typical disk thickness of CVD-diamond windows ($\varepsilon_r = 5.67$) is between 1.50 mm to 2.25 mm, which corresponds to a basic frequency(f_B) of 42 GHz and 28 GHz, respectively. The RF window with disk thickness of 1.861 mm is considered for this analysis. The reflection and transmission coefficient plots of this window are shown in Figure 2. The transmission bands of this window are at frequencies around 104 / 137 / 170 / 203 / 236 / 269 and 304 GHz which support multi-frequency operation at these frequencies. The modes for multi-frequency operation must have the same relative caustic radius in order to use the same quasi-optical launcher design (i.e. launcher radius, launcher cut length, and Brillouin angle) at different frequencies. Based on this study, the selected operating frequencies and their corresponding applications for different aspect ratios of DEMO [11-12] are listed in Table 2 along with the selected modes for the multi-frequency operation. Initially, the operating modes for 170 GHz and 203 GHz were suggested and successfully tested by the JAEA gyrotron team [20]. We have extended this mode series for the higher frequencies and suggest suitable modes for 236 GHz and 269 GHz. The relative caustic radii of all modes are nearly the same with only a small deviation of 0.08 % from the average value. Consequently, the suggested mode series has a high rating in the scheme discussed in [19].

Table 2. Properties of the selected operating modes of a multi-frequency hollow cavity gyrotron with 1.861 mm thick single disk CVD-diamond vacuum window.
(H = plasma heating, CD = current drive, A = DEMO aspect ratio)

Window transmision band (-20 dB) [GHz]	168.2-170.4	202.0-204.2	235.8-238.1	269.7-271.9
Applications	H (A=3.1)	H (A=3.6) CD (A=3.1)	H (A=4.0) CD (A=3.6)	CD (A=4.0)
Cavity mode	$TE_{-31,11}$	$TE_{-37,13}$	$TE_{-43,15}$	$TE_{-49,17}$
Mode eigenvalue	74.32	88.76	103.21	117.65
Relative caustic radius ($R_{caustic}/R_{cavity}$)	0.4171	0.4168	0.4166	0.4165
Normalized window thickness	5/2	6/2	7/2	8/2

2.3 Modes for frequency-step tunability

A Brewster-angle window has a significantly broad transmission bandwidth and its use is essential to achieve frequency-step tunability. The design and development of Brewster windows is ongoing for high-power, long-pulse gyrotrons [21]; however, otherwise tunable window systems could also be used for step-tuning. The proposed mode series for frequency-step tunability is shown in Table 3. These suitable modes around 236 GHz and over a 20 GHz bandwidth with steps of 2-3 GHz have a maximum relative caustic radius deviation of 3.5 % from the average value. All modes have the same rotation

since they will all use the same quasi-optical system. The detailed mode selection approach and step-frequency tunability of a 236 GHz DEMO gyrotron has been discussed in [22]. With a proper superconducting magnet design, it should be possible to achieve both multi-frequency operation and fast frequency-step tunability for a given tube.

Table 3. Suitable operating modes and their properties for a frequency-step tunable, hollow cavity gyrotron. Frequency steps: $\Delta f = 2$ - 3 GHz.

Frequency [GHz]	227.4	230.3	233.1	236.1	238.9	241.8	243.9
Δf [GHz]	2.9	2.8	2.9	-	2.9	2.9	2.0
Cavity mode	$TE_{-40,15}$	$TE_{-41,15}$	$TE_{-42,15}$	$TE_{-43,15}$	$TE_{-44,15}$	$TE_{-45,15}$	$TE_{-43,16}$
Relative caustic radius	0.402	0.407	0.412	0.417	0.421	0.427	0.403

3 Cavity design

3.1 Systematic cavity design approach

In this Section, a systematic hollow cavity design approach towards a 236 GHz gyrotron is discussed in details. However, this design approach is general and can be applicable to any hollow cavity design, independent to selected operating mode and frequency.

The cavity is the key component of a gyrotron in which its helical electron beam interacts with and transfers a part of its kinetic energy to a TE wave. The geometry of the optimized conventional cavity is shown in Figure 3. It is a cylindrical-symmetric structure with a straight midsection, a down-taper section and an up-taper section. To reduce unwanted mode conversions due to abrupt discontinuities, adjacent sections are connected via parabolic smoothing. The radius of the straight section can be estimated using Equation 1, which implies operation close to the cutoff frequency with the desired TE mode. All the other physical parameters have to be optimized to obtain an appropriate field profile with the required value of the quality factor Q.

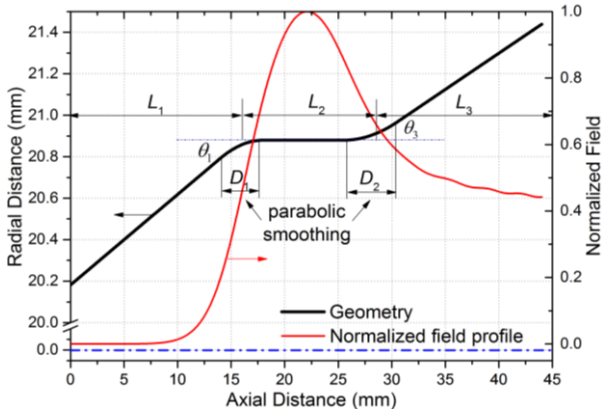

Figure 3: Geometry of the conventional design for a DEMO gyrotron cavity with the longitudinal field profile of the operating mode.

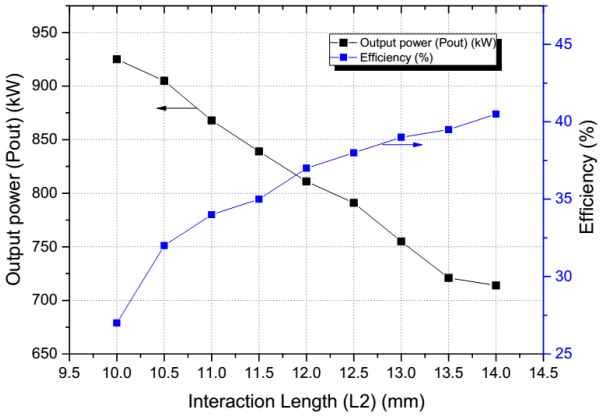

Figure 4: Output power and efficiency of cavity with various interaction section lengths (L_2) from 10 mm to 14 mm. Operating parameters for any particular interaction length are listed in table 4.

The calculated cavity radius for the $TE_{43,15}$ mode at 236 GHz is 20.88 mm and the electron beam radius for maximum coupling is 9.06 mm. As per the current technological possibilities, a maximum wall loading of 2 kW/cm^2 has been considered for the cavity design. The midsection length L_2 is a major factor of the cavity performance. Our parametric analysis of L_2 is presented in Figure 4. For various lengths, the cavity performance is determined with the help of the self-consistent code SELFC in the in-house CAVITY package [23]. At the beginning, all the other geometry parameters were estimated from previous experiences of the cavity design for the W-7X (140 GHz) and ITER (170 GHz) gyrotrons. The initially selected values of these parameters were: $L_1 = L_3 = 16$ mm, $\theta_1 = \theta_3 = 2.5°$, $D_1 = D_2 = 5$ mm. Given these values, the gyrotron operating parameters (e.g. magnetic field, beam current, beam energy)

were optimized for each L_2 (see Table 4). A reasonable value of $\alpha = 1.25$ was assumed for the pitch factor (ratio of transverse to axial electron velocity). Here, It is clear from the results that the interaction efficiency of the gyrotron increases monotonically with the mid-section length: The diffractive quality factor Q_{diff} of the cavity increases with the cavity length, which supports the increase in the interaction efficiency.

Table 4. Operating parameters and performance of the cavity for several midsection lengths. The operating parameters are selected for maximum efficiency considering target wall loading $\rho_{\mathrm{pk,max}}$.

Midsection length L_2 [mm]	10	10.5	11	11.5	12	12.5	13	13.5	14
Magnetic field [T]	9.37	9.20	9.17	9.15	9.13	9.10	9.09	9.07	9.05
Beam current [A]	48	45	43	40	38	36.5	35	33.5	33
Beam electron energy [keV]	72	62	60	59	58	56.5	55.5	54.5	53.5
Diffractive quality factor Q_{diff}	961	1066	1179	1299	1429	1566	1712	1868	2033
Wall loading [kW/cm^2]	2.01	1.98	2.00	2.00	1.99	2.02	1.99	2.00	2.01
Output power [kW]	925	905	868	839	811	792	756	721	715
Interaction efficiency [%]	26.8	32.5	33.6	35.6	36.8	38.3	38.9	39.5	40.5

The ohmic wall-loading of the cavity can be calculated using [24]:

$$P_{\Omega} \approx \frac{Q_{\mathrm{diff}} \cdot P_{\mathrm{out}}}{Q_{\Omega} \cdot S} \propto \frac{P_{out} \cdot L_2 \cdot \delta}{\lambda^2 \cdot {R_{cavity}}^2 \cdot (1 - m^2/{\chi_{m,p}}^2)} \tag{3}$$

Where Q_{Ω} is the ohmic quality factor of cavity, S is the cavity wall area and $\delta = \sqrt{(2 \,/\, \sigma\, \omega\, \mu)}$ is the skin depth. Here, we used the typical value of effective conductivity $\sigma = 1.4 \cdot 10^7$ S/m (to be compared to the value $\sigma_{\mathrm{Cu,0}} = 5.7 \cdot 10^7$ S/m for ideal copper at room temperature) to account for the expected conductivity reduction due to surface roughness and high operating temperature. The Ohmic wall loading increases with the cavity length due to increase in quality factor. This explains why, to keep the wall loading constant, it is necessary to reduce the input power, which consequently reduces the output power. The self-consistent time-dependent analysis using the CAVITY package with the consideration of main competing modes suggests a mid-section length of less than 13 mm, since with mid-section lengths of more than 13 mm, mode competition becomes crucial and it is very difficult to excite the main operating mode during diode start-up. After this investigation, $L_2 = 12$ mm was selected for further analysis, which is a good compromise between the demands for high output power, high efficiency and acceptable mode competition.

As a next step, the influence of the input and output angles on the gyrotron performance was analyzed. For $L_2 = 12$ mm and corresponding operating parameters, output power, efficiency and wall-loading are plotted in Figure 5, as a function of input and output angles. The result shows that with an output angle of 2.0º, instead of 2.5º, the output power can be increased from 811 kW to 824 kW with higher efficiency. The optimum point, achieving the maximum power and efficiency at wall loading < 2 kW/cm^2, is shown on the contour plots of Figure 5.

Lengths and smoothing regions of the input and output sections were studied with the scattering matrix codes from the CAVITY package, which calculate transmission and reflection coefficients of the possible modes. The input-taper section is designed such that the cutoff frequency of the input taper section is higher than the operating frequency (cf. Equation 1). Thus, it works as a reflector and helps the cavity to maintain the desired Q value. It turned out that with optimized design ($L_1 = 16$ mm, $D_1 = 4$ mm), more than 99 % of the $TE_{43,15}$ mode amplitude is reflected from the input section without spurious mode excitation. Concerning the up-taper section, transmission of mode $TE_{43,15}$ with more than 99 % is achieved with $L_3 = 16$ mm, $D_2 = 5$ mm.

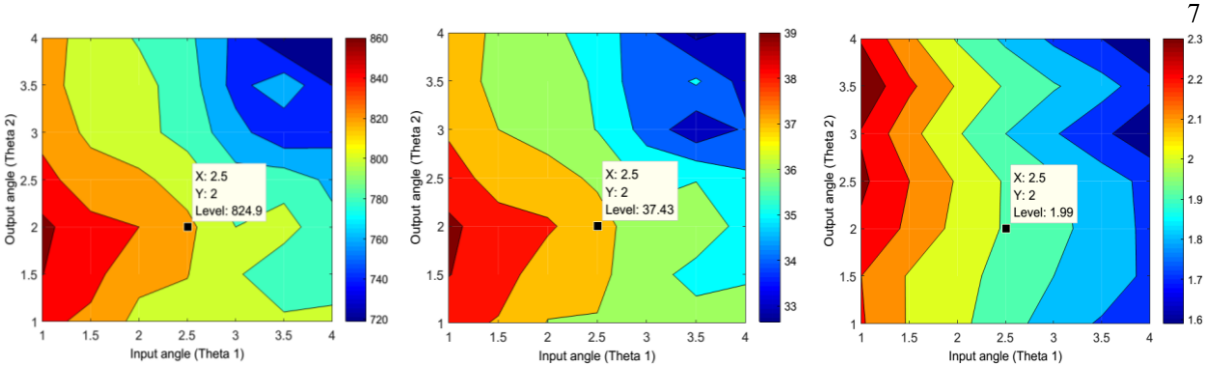

(a) (b) (c)

Figure 5: Effect of the input and output angles on (a) output power, (b) efficiency and (c) ohmic wall loading. The optimum point, together with the corresponding value, is indicated in each diagram.

Table 5. Final physical parameters of the 236 GHz cavity after systematic design approach.

Input taper			**Midsection**		**Output taper**		
Length L_1	Angle θ_1	Smoothing length D_1	Length L_2	Radius R_{cav}	Length L_3	Angle θ_2	Smoothing length D_2
16 mm	2.5°	4 mm	12 mm	20.88 mm	16 mm	2.0°	5 mm
D_1 and D_2 extend equally over L_1 and L_2, and L_2 and L_3, respectively, so the total cavity length is 44 mm.							

The finalized cavity parameters are listed in Table 5, and the geometry with the longitudinal field profile has already been shown in Figure 3. The ohmic quality factor (Q_Ω) and the diffractive quality factor (Q_{diff}) of the final cavity design is 62937 and 1443, respectively.The steps of the proposed systematic cavity design approach are summarized in Table 6.

Step 1: Calculate midsection radius and beam radius using standard formulas for the desired operating mode.
Step 2: Estimate initial geometrical cavity parameters (L_1, L_2, L_3, θ_1, θ_2, D_1, D_2) from the design goals, technical limitations, cold cavity profile and previous cavity design experiences.
Step 3: Simulate gyrotron interaction with various mid-section lengths L_2, keeping all other physical parameters fixed, and find the optimum value (e.g. Figure 4 and Table 4). The operating parameters (beam voltage, beam current, magnetic field, etc.) must be optimized for each particular L_2.
Step 4: Optimize input and output angles θ_1, θ_2 with regards to power and efficiency using the optimized mid-section length from step 3 and corresponding operating parameters (e.g. Figure 5).
Step 5: Optimize input taper section length L_1 and input smoothing length D_1 by calculating reflections of the RF modes from input section. These lengths should be set to obtain maximum reflection of the operating mode without mode conversion.
Step 6: Optimize output taper section length L_3 and output smoothing length D_2 to have maximum RF power transmission to the quasi-optical launcher without mode conversion.

Table 6: Steps of the systematic cavity design approach.

3.2 Performance impact of deviations from the selected geometrical parameters

To study the influence of each geometrical parameter on the cavity performance and to further verify the chosen geometry of Table 5, the output power and efficiency were calculated for parameters different from the chosen ones. Only one parameter was varied at a time. Such a study also gives information on the acceptable manufacturing tolerances. In this way, it was verified that the selected geometry is actually optimum, despite the fact that, during the design approach, the geometry parameters were fixed sequentially (i.e.one after the other), rather than simultaneously. The performance variation is shown in Table 7. Here, the definition of the percentage variation p of quantity X (output power P or efficiency η)

is given by Equation 4. However, when more than one physical parameters are changed, the total influence on the cavity performance is not simply equal to the sum of the individual ones. As one can see from Table 7, the midsection length L_2 has the largest impact on gyrotron performance. This justifies that it was the first parameter to address during the design procedure.

$$p_X = \frac{2 \cdot (X_{\max} - X_{\min})}{X_{\max} + X_{\min}} \cdot 100\ \% \tag{4}$$

Table 7. Influence of the individual geometrical parameters on the overall cavity performance.

Parameter	L_2	θ_1 and θ_2	D_1 and D_2	L_1 and L_3
Investigated range	10 – 15 mm	1° – 4°	1 – 4 mm	10 – 19 mm
Output power variation p_X	25.6 %	17.7 %	14 %	3.7 %
Efficiency variation p_X	40.7 %	16.7 %	12 %	4 %

4. Performance of the proposed cavity design

The detailed RF behavior of the proposed cavity is investigated to validate the physical design and find the most suitable operating parameters of the gyrotron. As discussed in Section 2, the mode $TE_{-43,15}$ (eigenvalue ≈ 103.2132) was selected as the operating mode. As it is of high order, its spectrum is quite dense (cf. Figure 1(a)), therefore it is especially important to identify start-up conditions and operating parameters to excite this mode with good stability margin. The simulations were performed using the in-house code packages CAVITY [23] and EURIDICE [25].

Initially, the operating point was refined for the final cavity design (Table 5) by single-mode simulations. The main selection criteria for operation parameters were: more than 35% of interaction efficiency, high output power and stable RF output. For optimum operation of the designed cavity, an axial magnetic field of 9.165 T at the cavity center is required with a beam current and beam electron energy of 43 A and 61 keV, respectively. assuming a pitch factor $\alpha = 1.25$. Instead of the typical $\sigma = 1.4 \cdot 10^7$ S/m, an updated conductivity value of $\sigma = 1.9 \cdot 10^7$ S/m was used for the cavity wall. This was done after more detailed considerations, which are described in Appendix 1.

As a next step, multi-mode, time-dependent, self-consistent simulations were performed to study the influence of the neighboring modes on the main mode operation. For a rigorous analysis, the 99 possibly relevant modes shown in Figure 1(a) were considered for the start-up simulation. The beam energy was raised from 20 keV to 61 keV linearly in the start-up phase, while the pitch factor varied adiabatically and the beam current varied according to the temperature-limited regime of a diode-type magnetron injection gun (MIG). The parameters were kept constant at their nominal values to check the stability of the operating point. In Figure 6, the start-up scenario considering an ideal electron beam (e.g. no velocity spread or radial width) is presented, as simulated by EURIDICE. Stable RF output of 960 kW with an interaction efficiency of 38 % has been achieved. As in usual gyrotron start-ups, modes having a high relative coupling (more than 0.8) and an operating frequency close to the design frequency (236 GHz, see Figure 1(a)) are excited in the start-up (time variable from 0 to 3000).

Due to practical limitations of a MIG, it is not possible to generate an ideal electron beam without velocity spread and radial width. Therefore, it is important to check cavity performance with an electron beam with velocity spread and radial width, henceforth termed *realistic beam*. For the cavity design presented here, the individual effects of velocity spread and radial width on the gyrotron performance are discussed in detail in [26]. The result for a realistic electron beam (6% perpendicular velocity spread, λ/4 radial width) is presented in Figure 7. In this case, stable RF-output has also been achieved, but with slightly lower output power of 920 kW and interaction efficiency of 36 %. During the simulation, the output power of all considered neighboring modes at the operating point remains at less than 0.1% of the operating mode power, which itself remains constant. This result indicates stable operation without spurious mode generation or mode loss.

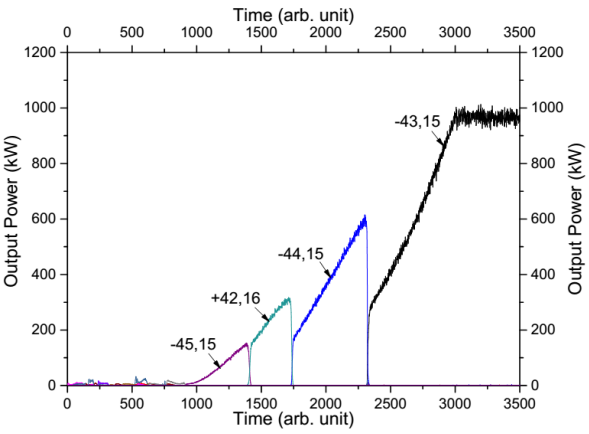

Figure 6: Start-up scenario considering 99 neighboring modes (shown in Figure 1(a)) and an ideal electron beam.

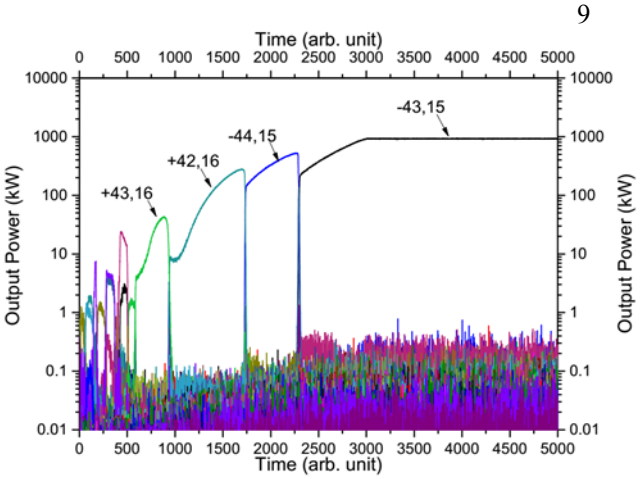

Figure 7: Start-up scenario for longer time duration, and with the realistic electron beam parameters. Beam energy linearly increases from 20 keV to 61 keV till t=3000 and remains constant till t=5000

It is desirable to have stable main mode operation not only with the nominal operating parameters, but also within a certain range of the operating parameters. This will further ensure robust operation during actual experiments. In Figure 8, the stability of the operation is shown with respect to the beam electron energy. The energy has been increased in steps of 0.1 keV from 61 keV until mode loss. From single-mode and multi-mode time-domain analyses by EURIDICE, it was verified that mode loss is only due the detuning and not because of mode competition [27]. With the suggested magnetic field of 9.165 T, the operating mode is stable up to the electron beam energy of 62.3 keV, i.e. there is a 1.3 keV margin with respect to the nominal beam energy. The stability margin of the tube operation can be extended by operating the gyrotron at higher magnetic field, which corresponds to lower detuning. Using a modified magnetic field of 9.177 T at the cavity center, a stability margin of up to 2 keV can be achieved. This, of course, comes at the expense of power and efficiency at the operating point, which are now reduced by 905 kW and 35%, respectively (see Figure 8(b)).

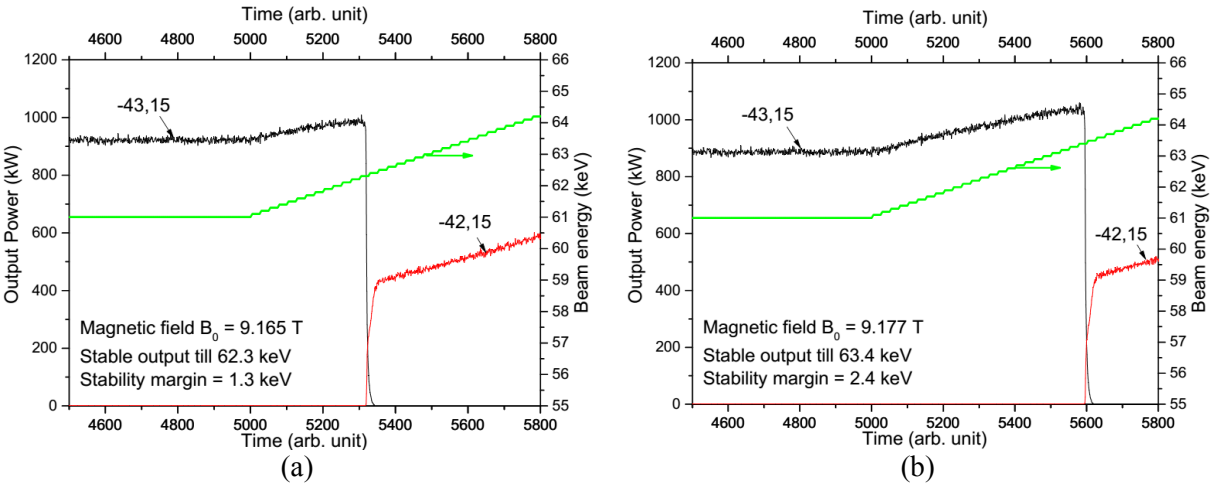

(a) (b)

Figure 8: Stability analysis of the operating point. The beam energy has been increased in 0.1 keV steps (a) with magnetic field of 9.165 T, (b) 9.177 T.

As discussed in Section 3, the cavity wall-loading is a major limiting factor for the output power of the DEMO gyrotron. If the ohmic loading limit of 2 kW/cm^2 was relaxed (i.e. if a more efficient cooling was used) than more power could be possible. This is illustrated in Table 8, where the Operating parameters, output power and efficiency for the same cavity geometry and with ideal beam parameters, but with higher wall loading are listed.. The result confirms the approximate proportionality between output power and peak wall loading suggested by Equation 3 and motivates possible improvements of the cavity cooling capabilities.

Table 8. Operating parameters and output power of 236 GHz gyrotron with higher wall loading.

Maximum wall loading (kW/cm^2)	Beam energy (keV)	Beam current (A)	Output power (kW)	Interaction efficiency (%)
2.00	61	43	960	38
2.18	65	45	1070	38
2.43	65	50	1200	38

Multi-frequency, multi-purpose operation of the proposed cavity design has been also validated with realistic multi-mode simulations like those presented above. The operating parameters were optimized for all four suggested frequencies of 170 GHz/ 203 GHz/ 236 GHz and 269 GHz. The results are summarized in Table 9.

Table 9. Multi-frequency operation of the proposed hollow cavity DEMO gyrotron. The frequency dependence of Glidcop conductivity is considered according to Appendix 1

Frequency (GHz)	**170.0**	**203.0**	**236.1**	**269.1**
Mode	$TE_{31,11}$	$TE_{37,13}$	$TE_{43,15}$	$TE_{49,17}$
Mode eigenvalue	74.325	88.769	103.213	117.656
Magnetic field [T]	6.785	7.975	9.165	10.349
Beam radius [mm]	9.13	9.10	9.06	9.04
Beam electron energy [keV]	81	70	61	55
Beam current [A]	59	48	43	38
Diffractive quality factor Q_{diff}	820	1171	1443	1839
Ohmic Wall loading [kW/cm^2]	2.00	1.99	2.00	1.99
Effective conductivity [10^7 S/m]	2.12	2.01	1.91	1.82
Without velocity spread or radial spread consideration				
Output power [kW]	1650	1220	960	821
Interaction efficiency [%]	35	37	38	40
With 6 % velocity spread and λ/4 radial width				
Output power [kW]	1550	1150	920	765
Interaction efficiency [%]	33	35	36	38

5. Conclusions

Physical design studies and analyses of DEMO-compatible advanced gyrotrons are under investigation at KIT. Gyrotrons having very high-order operating modes (eigenvalues > 100) are suggested to meet power and frequency requirements. Such modes can be selected according to multi-frequency operation and frequency tunability requirements. A generalized, systematic cavity design approach has been proposed and implemented for a $TE_{43,15}$-mode cavity at 236 GHz to ensure optimal interaction section design. Based on this, optimum operating parameters of the gyrotron have been found considering design goals and most possible technical limitations. Using the EURICIDE code, time-domain self-consistent simulations have been performed with 99 competing modes to verify cavity performance. Stable RF output of 920 kW could be achieved with interaction efficiency of 36%. With the suggested mode series, multi-frequency operation of the DEMO gyrotron has been estimated at 170 GHz / 203 GHz / 236 GHz and 269 GHz.

6. Acknowledgement

This work has been carried out within the framework of the EUROfusion Consortium and has received funding from the Euratom research and training programme 2014-2018 under grant agreement No 633053. The views and opinions expressed herein do not necessarily reflect those of the European Commission. Parts of the simulations presented in this work have been carried out using the HELIOS supercomputer at IFERC-CSC.

Appendix 1. Conductivity of a Glidcop cavity wall considering temperature and frequency dependency with surface roughness

Cavities made of the copper alloy Glidcop are used extensively in high power gyrotrons because of the advanced mechanical properties of this material. Based on measurements at Thales Electron Devices [28], a relation between the Glidcop conductivity and the temperature, $\sigma_G = f_G(T)$, was obtained. As the cavity wall thickness is many times larger than the skin depth, the effect of surface roughness can be calculated using the Hammerstad-and-Bekkadal formula [29-30], see Equation 5. Here, K_{sr} is the enhancement factor which is the ratio of wall losses power at a rough surface to the wall losses power at the corresponding smooth surface, h is the RMS height of the rough surface profile and δ is the skin depth, which depends on the angular frequency ω of the incident wave and the magnetic permeability μ of the material (see Equation 6)

$$K_{sr} \equiv \frac{P_{loss,rough}}{P_{\text{loss,smooth}}} = 1 + \frac{2}{\pi}\arctan\left(\sqrt{2}\left(\frac{h}{\delta}\right)^2\right) \tag{5}$$

$$\delta = \sqrt{\frac{2}{\sigma\,\omega\,\mu}} \tag{6}$$

The combined formula to calculate the effective conductivity of Glidcop $\sigma_{\text{Glidcop,eff}}$, considering the operating frequency, temperature dependency, and surface roughness is shown in Equation 8. For calculations in this paper, the typical values T=250 ℃, h = 0.1μm have been used.

$$\sigma_{\text{Glidcop,eff}} = \frac{f_G(T)}{\left[1 + \frac{2}{\pi}\cdot\arctan\left\{\frac{\omega\,\mu h^2}{\sqrt{2}}\cdot f_G(T)\right\}\right]^2} \tag{7}$$

8. References

[1] Thumm M. 2015 *State-of-the-art of high power gyro-devices and free electron masers, update 2014* Sci. Rep. KIT-SR 7693 (DOI: 10.5445/KSP/1000047012)

[2] Erckmann V. *et al* 2014 *AIP Conf. Proc.* (Sorrento, Italy) (DOI:10.1063/ 1.4864559)

[3] Kasugai A. *et al* 2008 Nucl. Fusion **48** 054009

[4] Denisov G. G. *et al* 2008 Nucl. Fusion **48** 054007

[5] Thumm M. 2014 *IEEE Trans. Plasma Sci.* **42** 590-99

[6] Litvak A. *et al* 2011 *Plasma Phys. Control. Fusion* **53** 124002

[7] Kalaria P. *et al* 2014 *IEEE Trans. Plasma Sci*. **42** 1522-28

[8] Poli E. *et al* 2013 *Nucl. Fusion* **53** 013011

[9] Franck J. *et al* 2014 *IEEE International Vacuum Electronics Conference* (Monterey, CA) (DOI: 10.1109/IVEC.2014.6857475)

[10] Thumm M. *et al* 2015 *International Journal of Terahertz Science and Technology* **8** 85-128 (DOI: 10.11906/TST.085-100.2015.09.09)

[11] Franke T. *et al* 2014 *Fusion Engineering and Design* **96-97** 468-472 (DOI:10.1016/j.fusengdes.2014.12.036)

[12] Garavaglia S. *et al* 2015 *AIP Conference* (California, USA) (DOI: 10.1063/1.4936546)

[13] Pagonakis I. Gr. *et al* 2008 *IEEE Trans. Plasma Sci.* **36**, 469-80

[14] Zhang J. *et al* 2016 *Nucl. Fusion* **56** 026002

[15] Jin J. *et al* 2013 *IEEE Trans. Plasma Sci.* **41** 2748-53

[16] Prinz O. *et al* 2009 *IEEE Trans. Elect. Devices* **56** 828-34

[17] Schmid M. *et al* 2015 *Fusion Engineering and Design* **96-97** 589-92

[18] Borie E. 1991 Review of Gyratron Theory, KFK-report 4898

[19] Franck J. *et al* 2015 *Nucl. Fusion* **55** 013005
[20] Sakamoto K. *et at* 2013 *IEEE International Vacuum Electronics Conference* (Paris, France) (DOI: 10.1109/IVEC.2013.6571137)
[21] Gantenbein G. *et al* 2014 *IEEE Trans. Elect. Devices* **61** 1806-11
[22] Kalaria P.C. et al 2016 10th German Microwave Conference (Bochum, Germany) (DOI: 10.1109/GEMIC.2016.7461635)
[23] Kern S. 1996 *Numerical Codes for interaction calculations in gyrotron cavities at FZK,* Proc. 21st Int. Conf. Infrared and Millimeter Waves, Berlin, Invited Paper AF2 and 1997 *Numerische Simulation der Gyrotron-Wechselwirkung (Numerical simulation of the gyrotron interaction)*, Scientific Report FZKA 5837, Karlsruhe.
[24] Nusinovich G. S. 2004 *Introduction to the Physics of Gyrotron*, The Johns Hopkins University Press, Maryland.
[25] Avramides K. A. et al 2012 17th Joint Workshop on Electron Cyclotron Emission and Electron Cyclotron Resonance Heating (Deurne, The Netherlands) (DOI: 10.1051/epjconf/20123204016)
[26] Kalaria P. C. et al 2015 IEEE International Vacuum Electronics Conference (Beijing, China) (DOI: 10.1109/IVEC.2015.7223769)
[27] Kalaria P. C. et al 2016 IEEE International Vacuum Electronics Conference (Monterey, USA)
[28] Bariou D. *et al* 2007 *Design report ITER 170 GHz Gyrotron Contract No. EFDA-03/960*. Internal Report, Thales Electron Devices, RT5307
[29] Hammerstad E. O. *et al* 1975 *Microstrip Handbook* , Univ. Trondheim, Norway.
[30] Leung T. *et al* 2010 IEEE trans. Advanced Packaging **33** 839-56